JOURNAL OF SPACECRAFT AND ROCKETS
Vol. 41, No. 2, March–April 2004

X-38 Experimental Aeroheating at Mach 10

Scott A. Berry,* Thomas J. Horvath,* K. James Weilmuenster,† Stephen J. Alter,‡ and N. Ronald Merski Jr.†
NASA Langley Research Center, Hampton, Virginia 23681

Details are provided of a recent effort at the NASA Langley Research Center to extend the experimental aeroheating database for the X-38 program to higher-Mach-number conditions. Global surface heat-transfer distributions were measured on 0.0177- and 0.0236-scale models of the proposed X-38 Rev 8.3 configuration at Mach 10 in air. The parametrics that were investigated primarily include freestream unit Reynolds numbers of 0.6 to 2.2 $\times$ 10^6/ft and body-flap deflections of 15, 20, and 25 deg for an angle of attack of 40 deg. The model-scale variance was tested to obtain laminar, transitional, and turbulent heating levels on the deflected body flaps. In addition, a limited investigation of forced boundary-layer transition through the use of discrete roughness elements was performed. Comparisons of the present experimental results to computational predictions and previous experimental data were conducted. Laminar, transitional, and turbulent heating levels were observed on the deflected body flap, which compared favorably to the computational results and to the predicted heating based on the flight aerothermodynamic database.

Nomenclature

F	=	correlation constant
H	=	enthalpy, BTU/lbm
h	=	heat-transfer coefficient (lbm/ft^2-s), $= \dot{q}/(H_{\text{aw}} - H_w)$ where $H_{\text{aw}} = H_{t2}$
k	=	trip height, in.
L	=	reference length taken from nose to end of body
M	=	freestream Mach number
N	=	correlation exponent
P	=	pressure, psia
$\dot{q}$	=	heat-transfer rate, BTU/ft^2-s
Re	=	unit Reynolds number, 1/ft
T	=	temperature, °R
t	=	time, s
v	=	velocity, ft/s
x, y	=	Cartesian coordinates
α	=	angle of attack, deg
δ_{BF}	=	body-flap deflection, deg
ρ	=	density, slugs/ft^3

Subscripts

FR	=	Fay–Riddell stagnation point reference
Ref	=	reference value ahead of body-flap separation, $x/L = 0.75$
$t1$	=	reservoir conditions
$t2$	=	stagnation conditions behind normal shock
w	=	wall
∞	=	freestream conditions

Introduction

THE crew return vehicle (CRV), as envisioned by NASA, will provide emergency return-to-Earth capability from the International Space Station (ISS) in the event of medical or mechanical problems and shuttle nonavailability.[1] Figure 1 provides an artist's rendering of the CRV docked to the ISS for use in an emergency. The X-38 program led by NASA Johnson Space Center (JSC) sought to fly a full-scale technology demonstrator to validate key design and operational aspects for the CRV.[2] The X-38 technology demonstrator mission, which was planned for the early 2003 time frame, called for a 28.5-ft-long vehicle (designated as V201) to be released by a U.S. Space Shuttle Orbiter from a high inclination orbit. Following the jettison of a deorbit engine module, the X-38 was to return unpowered (similar to the space shuttle) and then deploy and use a steerable parafoil, a technology first developed by the U.S. Army, for its final descent.[3] Landing was to be accomplished on skids rather than wheels. Consistent with the X-38 program's goal to take advantage of available equipment and technology to reduce vehicle development costs by an order of magnitude,[4,5] the shape of the X-38 drew upon a synthesis of work performed by the U.S. government and industry over the last few decades.[6,7] The initial X-38 shape proposed by NASA JSC was based on a lifting-body concept originally developed and flown during the U.S. Air Force's PRIME (X-23/SV-5D) and PILOT (X-24A) projects in the mid-1960s and early 1970s.[8] The X-24A lifting-body shape was selected for the CRV mission because of its relatively high hypersonic lift-to-drag ratio (L/D) and volumetric efficiency and was designated as the X-38 Rev 3.1 configuration. The higher L/D translates to larger cross range capability and shorter loiter times in orbit. The current shape (Rev 8.3) departs from the X-23/X-24A and the initial Rev 3.1 in that it reflected changes to the vehicle upper surface to provide for more internal volume and structural stiffness to satisfy launch loads (for possible launch atop of an expendable rocket). High approach speeds and long roll-out distances associated with the low subsonic L/D characteristics from this lifting body required that the landing be augmented with a steerable parafoil.[9] Critical for injured or incapacitated crew, this method permited the CRV to land within close proximity of medical facilities with minimal reentry g loads.

Under a NASA/European partnership Daussault Aviation served as the prime contractor for development of X-38 flight databases. References 10–12 provide recent examples of this joint effort to derive the X-38 aerothermodynamic database (ATDB). The role of the NASA Langley Research Center (LaRC) Aerothermodynamics Branch has been to provide hypersonic laminar and turbulent global surface heating and aerodynamic force and moment data for CFD validation and to complement data obtained in European facilities. Results from early LaRC wind-tunnel heating tests of the Rev 3.1 configuration compared favorably to CFD computations.[13,14] Boundary-layer transition data were obtained,[15] which could be compared to similar shuttle measurements[16] in order to support the use of a Re_θ/M_e transition criterion. This criterion is intended to be

Presented as Paper 2001-2828 at the AIAA 35th Thermophysics Conference, Anaheim, CA, 11–14 June 2001; received 24 July 2001; revision received 3 January 2003; accepted for publication 17 January 2003.

*Aerospace Technologist, Aerothermodynamics Branch, Aerodynamics, Aerothermodynamics, and Acoustics Competency.
†Aerospace Technologist, Aerothermodynamics Branch, Aerodynamics, Aerothermodynamics, and Acoustics Competency. Associate Fellow AIAA.
‡Aerospace Technologist, Aerothermodynamics Branch, Aerodynamics, Aerothermodynamics, and Acoustics Competency. Senior Member AIAA.

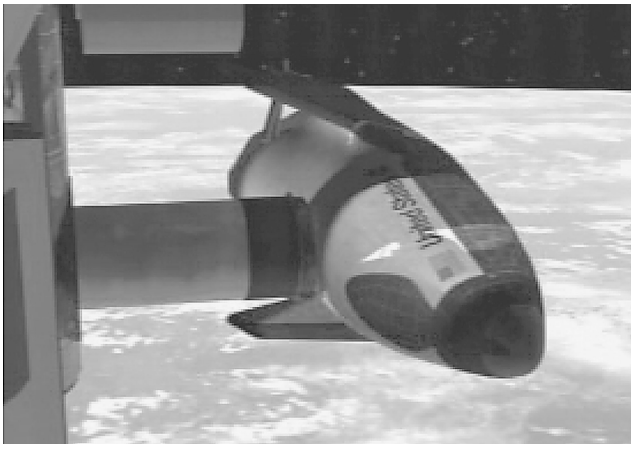

Fig. 1 X-38 as a lifeboat for the International Space Station.

used in the assessment of manufacturing tolerances (step and gaps) of the thermal-protection-system tiles.[12] Hypersonic aerodynamic screening studies on Rev 3.1 were conducted at LaRC to assess real-gas effects.[17] Reference 18 recently provided an overview of LaRC's contributions to the X-38 program. Since the time of these publications, additional aeroheating tests have been completed specifically to characterize the heating levels expected on the deflected body flaps under laminar, transitional, and turbulent conditions.

The thermal environment associated with the X-38 body flaps is considered a challenge from a design perspective because of the complex three-dimensional flowfield and resulting high surface temperatures anticipated in flight. The heating on the X-38 body flap will likely be influenced by three-dimensional flow separations and reattachments, shear-layer transition, multiple shock processing of the flow (bow, separation, reattachment), flow expansion, and acceleration over the flap edges and through the split gap, etc. As the X-38 flaps are designed as a hot structure,[19,20] the windward surface temperatures will produce a significant radiative heating exchange between the backside of the flap and aft cavity surfaces. The presence of critical component hardware in this region (e.g., flap actuator rod, flap seal) requires an accurate prediction of the environment to ensure proper performance and adequate thermal protection.

Early estimates of flap thermal loads at nominal conditions were based on fully catalytic, turbulent flow.[21] The actual flap design thermal environment that evolved from these early estimates accounted for additional factors such as vehicle weight growth and higher heating levels associated with a transitional reattaching boundary layer (the "transitional overshoot"). Based on nominal design flight conditions, it was felt that adequate margins existed. These thermal margins were significantly reduced when the operational environment was updated to include trajectory dispersions.

The X-38 program has undertaken a comprehensive computational and experimental effort to predict more accurately the heating environment associated with the windward surface of the deflected body flaps and to ensure thermal margins are not exceeded. Under the present NASA/European partnership previous Mach 6 windward flap heating measurements provided by LaRC were utilized to complement test results obtained in European facilities. The heating distributions on the flap windward surface were used for developing a thermal design model and flight scaling factors applicable to this localized region.[11] The present Mach 10 experimental measurements and corresponding numerical simulations are intended for refinement of this model and to reduce uncertainties.

This purpose of this paper is to present details of the recent effort at LaRC to extend the experimental aeroheating database for the X-38 program to higher-Mach-number conditions. Over 50 wind-tunnel runs have been completed in the LaRC 31-Inch Mach 10 Air Tunnel to characterize the state of the reattaching boundary layer on the deflected body flaps of Rev 8.3 configuration. The thermographic phosphor technique, which provides global surface heating images, was used to determine heating levels on the body flaps for angle-of-attack and body-flap deflections representative of expected flight conditions. Parametrics tested and presented here include a range of unit Reynolds numbers of 0.6 to 2.2×10^6/ft and body-flap deflections of 15, 20, and 25 deg for an angle of attack of 40 deg. These experimental results were complemented with laminar and turbulent computational predictions at wind-tunnel conditions of $Re = 0.6 \times 10^6$/ft and 2.2×10^6/ft for $\alpha = 40$ deg and $\delta_{BF} = 20$ deg.

Experimental Method

Model Description

A sketch of the X-38 Rev 8.3 vehicle is shown in Fig. 2. Three model scales have been built: 0.0177, 0.0236, and 0.0295, which correspond to 6-, 8-, and 10-in. length models, respectively. A rapid prototyping technique was used to build resin stereolithography (SLA) models for each scale, each with interchangeable body flaps. The SLA models were then assembled with the desired body-flap settings and used as a pattern to create molds from which the ceramic heating models were cast. Symmetric body-flap deflections of 15, 20, and 25 deg were selected based on consideration of the expected deflections in flight. To minimize conduction effects, the body flaps were thickened on the backside to 0.25 in. The flow-through gap between the port and starboard body flaps was maintained. To obtain accurate heat-transfer data using the one-dimensional heat-conduction equation, the cast models were made of a silica ceramic material with low thermal diffusivity and well-defined, uniform, isotropic thermal properties. The models were then coated with a mixture of phosphors suspended in a silica-based colloidal binder. The coatings do not require refurbishment between runs in the wind tunnel and have been measured to be approximately 0.001 in. thick. Boundary-layer trips, as shown in Fig. 2, were used for selected runs to ensure nonlaminar heating levels and consisted of a row of seven diamond-shaped trips, 0.0075 in. high by 0.1 in. square, placed nearly tip-to-tip at the $x/L = 0.368$ location. The trip elements were constructed of multilayered tape as discussed in Refs. 15 and 16 and sized based on prior experience.

Facility Description

The models were tested in the 31-Inch Mach 10 Air Tunnel of the Langley Aerothermodynamic Laboratory. A detailed description of this blowdown facility, which utilizes dried, heated, and filtered air as the test gas, is provided in Refs. 22 and 23. Typical operating conditions for the Mach 10 tunnel are stagnation pressures ranging from 350 to 1450 psia and stagnation temperatures from 1350 to 1450°F yielding freestream unit Reynolds numbers from 0.6 to 2.2×10^6/ft. The tunnel has a closed 31×31 in. test section with a contoured three-dimensional water-cooled nozzle to provide a Mach-number range from 9.6 to 10. A side-loading, hydraulically operated model injection mechanism can place the model into the flow in 0.6 s. Figure 3 is a photograph of the sting-mounted 0.0236-scale X-38 model in the tunnel.

Test Conditions

Flow conditions for the 31-Inch Mach 10 Air Tunnel were based on measured reservoir pressures and temperatures and a recent

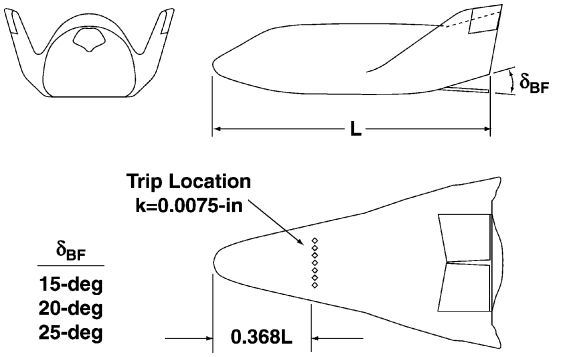

Fig. 2 Sketch of X-38 Rev 8.3 model.

Table 1 Nominal flow conditions for LaRC 31-Inch Mach 10 Air Tunnel

Re_∞ ($\times 10^6$/ft)	$M\infty$	Pt1, psi	Tt1, °R	Ht1, BTU/lbm	Pt2, psi
0.6	9.7	350	1770	442	1.2
1.1	9.8	720	1820	457	2.4
2.2	9.9	1450	1820	458	4.5

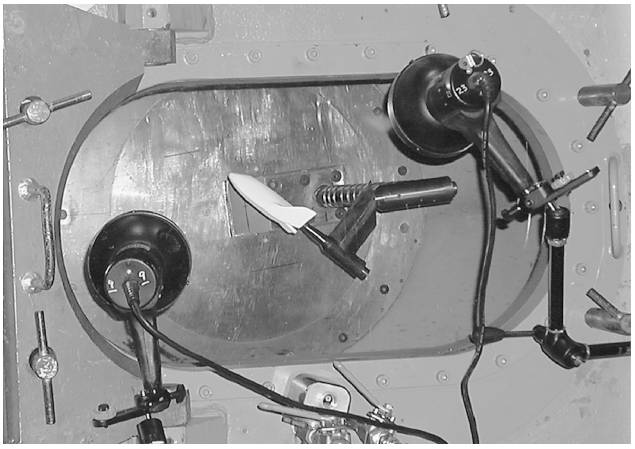

Fig. 3 Photograph of the X-38 model installed in the LaRC 31-Inch Mach 10 Tunnel.

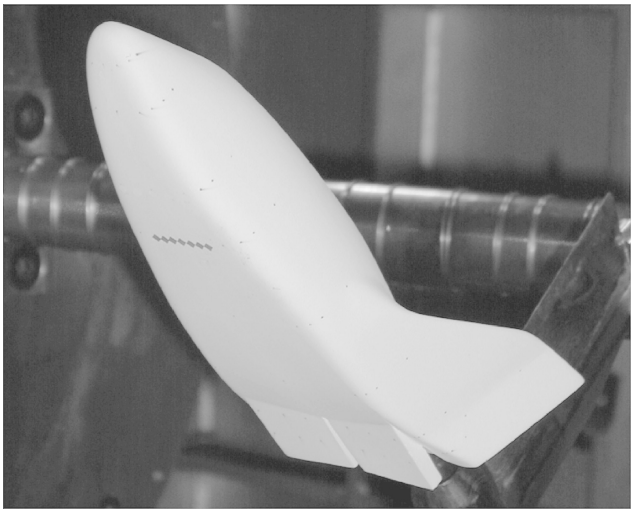

Fig. 4 Photograph of model showing boundary-layer trips on windward surface.

unpublished calibration of the facility. The different model configurations (with varying model scale and body-flap deflections) were tested at $\alpha = 40$ deg. A laser alignment system in conjunction with the fiducial marks located along the centerline of the model was used to ensure that zero sideslip was maintained. A limited number of runs were completed with boundary-layer trips, as shown in Fig. 4. These runs were made to ensure fully turbulent boundary-layer reattachment on the deflected body flaps using an established tripping method.[15,16] The nominal flow conditions for the 31-Inch Mach 10 Air Tunnel are listed in Table 1, which allows for an Re_L slightly less than the 3.8×10^6 for Mach 10 flight conditions (based on the X-38 trajectory information discussed in Ref. 18).

Test Techniques

The rapid advances in image-processing technology occurring in recent years have made digital optical measurement techniques practical in the wind tunnel. One such optical acquisition method is two-color relative-intensity phosphor thermography, which is currently being applied to aerothermodynamic testing in LaRC hypersonic wind tunnels. References 24–26 provide details about the phosphor thermography technique, and Refs. 15, 16, and 18 provide recent examples of the application of this technique to wind-tunnel testing. With this technique ceramic wind-tunnel models are fabricated and coated with phosphors, which fluoresce in two regions of the visible spectrum when illuminated with UV light. (Note the UV lights shown in Fig. 3 that illuminate the side of the model.) The fluorescence intensity is dependent upon the amount of incident UV light and the local surface temperature of the phosphors. By acquiring fluorescence intensity images with a color video camera of an illuminated phosphor model exposed to flow in a wind tunnel, surface temperature mappings can be calculated on portions of the model that are in the camera field of view. In this case the camera is located below the tunnel along with several UV lights to illuminate the model windward surface.

A temperature calibration of the system conducted prior to the test provides look-up tables used to convert the ratio of green and red intensity images to global temperature mappings. With temperature images acquired at different times during a wind-tunnel run, global heat-transfer images are computed assuming one-dimensional heat conduction. Phosphor thermography is routinely used in LaRC hypersonic facilities because models can be fabricated much quicker and more economically than more conventional techniques and can provide quantitative global heating information.

Data Reduction and Uncertainty

Heating rates were calculated from the global surface temperature measurements using one-dimensional, semi-infinite, solid heat-conduction equations.[25,26] Based on Ref. 26, the heat-transfer measurements are believed to be accurate to better than $\pm 15\%$. Heating distributions are presented in terms of the ratio of enthalpy-based heat-transfer coefficients h/h_{FR}, where h_{FR} corresponds to the Fay and Riddell[27] stagnation-point heating to a sphere with radius equal to the X-38 nosecap in the plane of symmetry. Repeatability for the normalized centerline heat-transfer measurements was found to be generally better than $\pm 8\%$.

Computational Method

Prediction Technique

The Langley Aerothermodynamic Upwind Relaxation Algorithm (LAURA)[28–30] was used for the computations presented in this paper. The LAURA code provided laminar and turbulent solutions of the thin-layer Navier–Stokes equations. The inviscid first-order flux is constructed using the flux-difference-splitting scheme of Roe[31] and entropy fix of Harten[32] with second-order corrections based on the symmetric total-variation-diminishing scheme of Yee.[33]

Turbulence Model

The turbulence model utilized in LAURA for the present study is based on the two-equation, k–ω model of Wilcox.[34] These equations are fully coupled to the equations for conservation of mass, momentum, and energy and are implemented to the surface boundary; wall functions are not used. The grid-adaptation routine within LAURA is applied to properly resolve the near-wall region. The ratio of production to dissipation in the model is limited from above and below by 20 and 0.05, respectively.

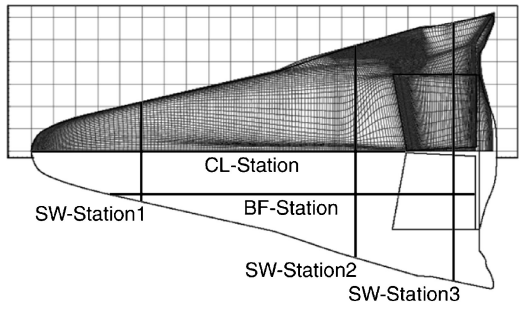

Fig. 5 Surface grid and body cut locations.

Boundary Conditions

The usual no-slip boundary condition for viscous flow is applied at the wall. The wall temperature was set at a constant value of 540°R, whereas freestream conditions are set at points on the outer boundary of the computational domain. The exit plane is set so that the outflow is supersonic.

Grid Generation

The surface grid for the X-38 Rev 8.3 configuration was constructed from CAD surfaces provided by NASA JSC using GRIDGEN[35] and VGM[36] and is shown in Fig. 5 along with the body cut locations used for experimental and computational comparisons. The volume grid was constructed using 3DGRAPE/AL.[37] The 20-deg body-flap deflection case was selected for computations. The expected nominal range of body-flap deflections during the hypersonic portion of reentry is 14 to 21 deg. Of the two experimental cases within this range, the 20-deg case was more likely to need verification against laminar computations. To simplify the grid geometry, the body flap was modeled as a wedge in order to eliminate the complexity behind the flap. However, because of the flow-through gap between the port and starboard flaps, a large number of grid points were concentrated near the centerline (as shown in Fig. 5) on the forebody in order to adequately define the gap region. Because slideslip is not considered in this report, only half the configuration is used in the computations. Grid-sensitivity studies were conducted, in a manner consistent with past experience,[38–40] first starting with a volume grid of $297 \times 341 \times 65$ and conducting two levels of grid coarsening in regions of higher gradients. The initial grid was sufficient to resolve the separation region at the flap hinge line and the viscous layer at the wall where the cell Reynolds number is of the order (1). The cell stretching at the edge of the viscous layer is less than 1.2.

Computational Conditions

For laminar solutions the freestream conditions for the 31-Inch Mach 10 Tunnel (Table 1) for both $Re = 0.6$ and 2.2×10^6/ft were used. A turbulent solution was obtained for the $Re = 2.2 \times 10^6$/ft freestream conditions starting at $x/L = 0.07$ on the body. Computations of wind-tunnel conditions are based on the assumption of air as a perfect gas.

Results and Discussion

Global Heating Images

The effect of Reynolds number and boundary-layer trips on the windward surface heating images for the 0.0236 scale model at an angle of attack of 40 deg is shown in Figs. 6–8 for body-flap deflections of 15, 20, and 25 deg, respectively. For the nontrip cases the heating levels on the forebody, as well as the size of the separation

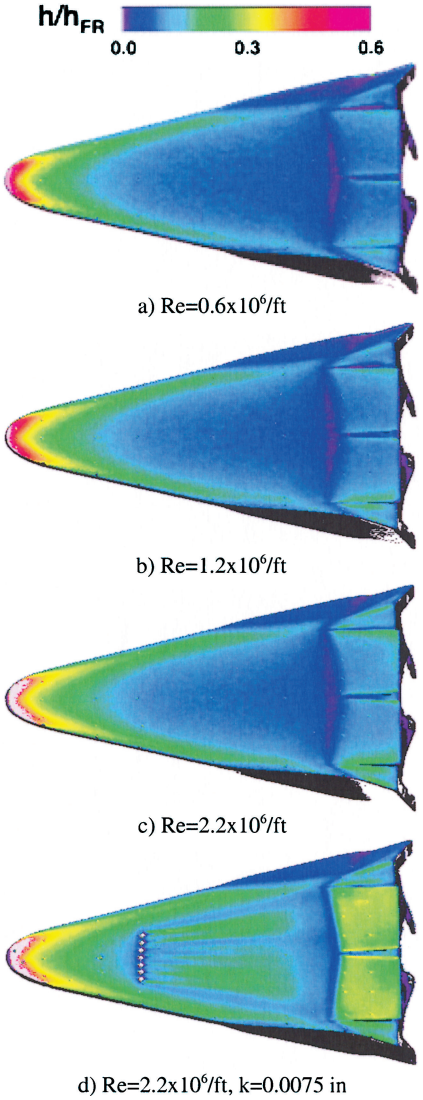

Fig. 6 Effect of unit Reynolds number and trips on global heating for $M_\infty = 10$, $\alpha = 40$ deg, and $\delta_{BF} = 15$ deg.

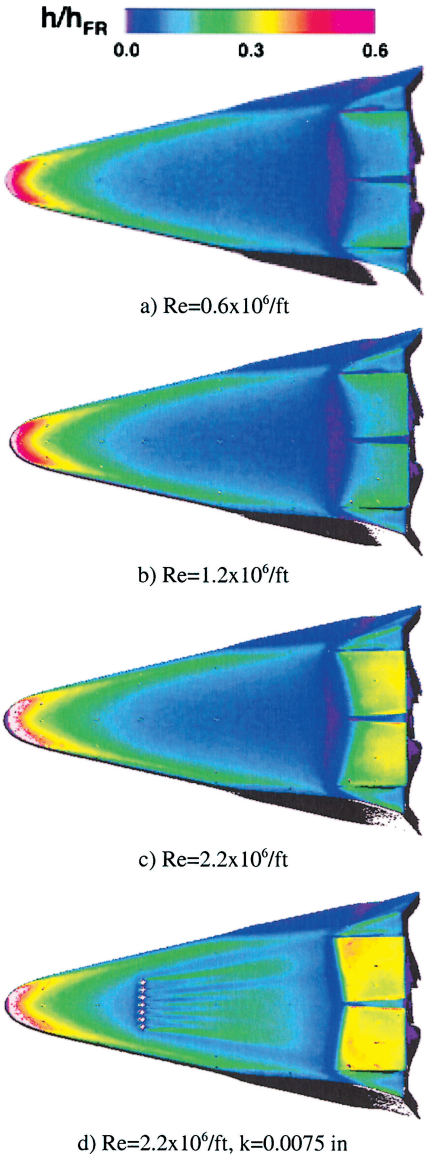

Fig. 7 Effect of unit Reynolds number and trips on global heating for $M_\infty = 10$, $\alpha = 40$ deg, and $\delta_{BF} = 20$ deg.

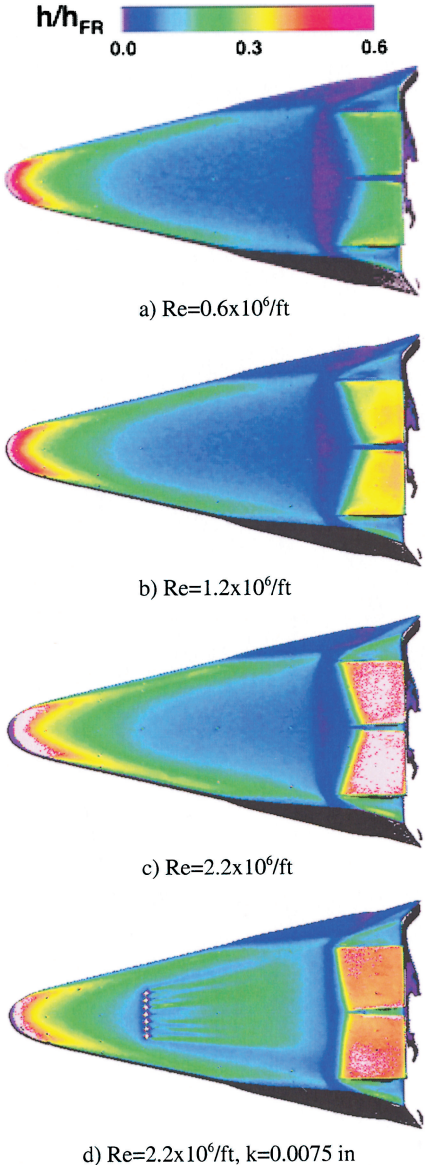

Fig. 8 Effect of unit Reynolds number and trips on global heating for $M_\infty = 10$, $\alpha = 40$ deg, and $\delta_{BF} = 25$ deg.

region in front of the deflected body flaps, remain essentially constant as the Reynolds number is increased for each body-flap configuration. This observation provides an indication that the attached forebody flow is laminar. However, for a given body-flap deflection the heating levels on the deflected body flap generally increase as the Reynolds number is increased, which suggests that the reattaching flow is mostly nonlaminar. For instance, for $\delta_{BF} = 20$ deg (Fig. 7) the heating level on the body flap is nearly identical for the two lowest Reynolds numbers (suggesting laminar reattachment), but has increased significantly at the highest Reynolds number (suggesting nonlaminar reattachment).

To ensure turbulent heating levels on the deflected body flaps, boundary-layer trips were used to force transition on the forebody ahead of the flap separation region. These trip cases, shown in Figs. 6d, 7d, and 8d ($k = 0.0075$ in trips and a Reynolds number of 2.2×10^6/ft), clearly show the nonlaminar flow downstream of the trips and the resulting reduction in the separation region size caused by the energized boundary layer. In addition, the body-flap reattachment heating appears to move closer to the hinge line. For the largest body-flap deflection tested, the trips appear to lower the heating on the body flaps compared to the untripped case (compare Figs. 8c and 8d). This trend was also observed in the LaRC 20-Inch Mach 6 Tunnel, where the larger body flap deflections tested provided evidence of a transitional overshoot.[15] Specifically, the body-flap heating was highest when the forebody remained laminar and transition occurred in the shear layer in front of the deflected body flap just prior to reattachment.

Forebody Heating Distributions

The LAURA code was used to provide laminar and turbulent heating predictions for the $\alpha = 40$ deg and $\delta_{BF} = 20$ deg case. A comparison of these predictions to the experimental measurements on the X-38 forebody is provided in Fig. 9. The experimental data

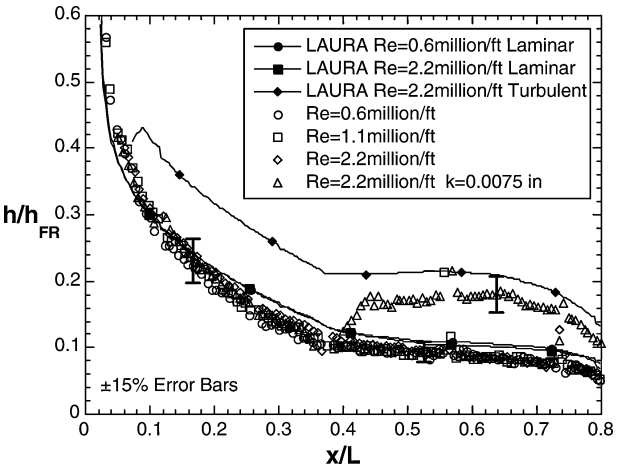

a) Centerline distribution

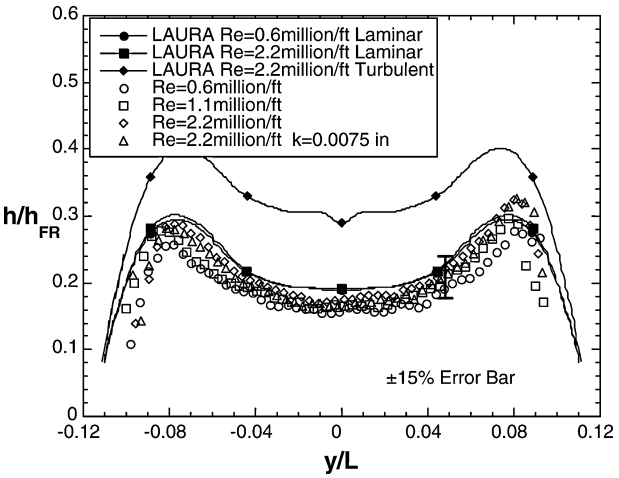

b) Spanwise distribution at SW-Station 1

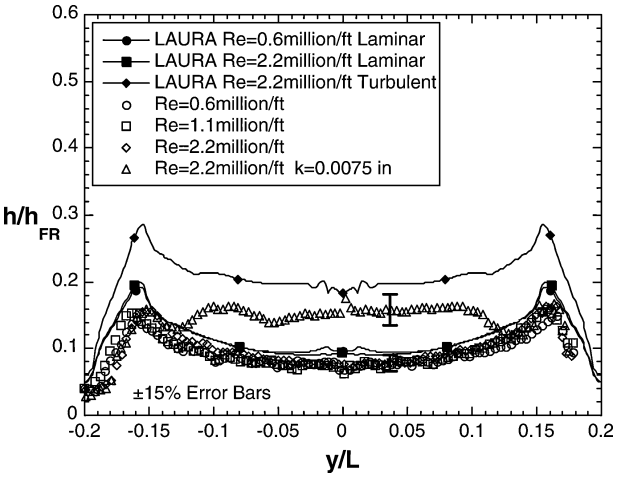

c) Spanwise distribution at SW-Station 2

Fig. 9 Comparisons of forebody heating results to predictions for $M_\infty = 10$, $\alpha = 40$ deg.

correspond to Reynolds numbers of 0.6, 1.1, and 2.2×10^6/ft, and the trip case ($k = 0.0075$ in at $x/L = 0.368$) at $Re = 2.2 \times 10^6$/ft. A ±15% error bar has been place on the experimental data in order to assess the comparisons.

The centerline distribution (Fig. 9a) shows the experimental heating levels to be within 15% of the laminar predictions for the cases without a boundary-layer trip. For the tripped case the turbulent computational results downstream of the trip location are slightly higher than the 15% error bar on the experimental data. Similar results are shown in the comparisons for the spanwise locations (SW-Stations 1 and 2 in Fig. 5). Figure 9b provides the heating distribution at SW-Station 1, which is ahead of the boundary-layer trips, and shows all four experimental results to be within 15% of the laminar computation. At SW-Station 2 (Fig. 9c), which is just ahead of the separated flow region, the laminar solution is within 15% of the untripped cases, whereas the tripped case remains below the turbulent prediction. The boundary-layer trips appear to be effective, as transition onset is immediate. Furthermore, the plateau of the heating level downstream of the trip suggests that fully turbulent flow was achieved. However, without further evidence of the validity of either the experimental or computational results, the only conclusion that can be reached about the tripped case is that the flow is nonlaminar on the forebody. Note that both the laminar and turbulent computations at SW-Station 2 provide evidence of perturbations near centerline that appear to be related to the high concentration of grid points noted earlier and shown in Fig. 5.

Body-Flap Heating Distributions

A comparison of the body-flap heating is provided through distributions at BF-Station and SW-Station 3 (as shown in Fig. 5). Figure 10 provides a comparison of the experimental results to predictions at these locations for the $\delta_{BF} = 20$ deg case. The measured heating for the $Re = 0.6 \times 10^6$/ft case is shown to agree in both magnitude and distribution to the laminar predictions on the body flap in both the longitudinal cut (Fig. 10a) and the spanwise cut (Fig. 10b). Note that the disparity between measurement and prediction for x/L of 0.2 to 0.4 is caused by the phosphor data that have not been spatially corrected for surface curvature using the IHEAT code Map3D tool first discussed in Ref. 18. This mapping technique would have permitted a more accurate spatial representation of the global data, especially for regions of high surface curvature towards the outer edges of the global images, for extraction and comparison to the predictions. However, aside from the leading edge of the model the measured laminar heating data are within the experimental uncertainty of the laminar predictions. For the highest-Reynolds-number case (without trips) the heating on the body flap approaches the level of the turbulent predictions towards the end of the body flap, whereas the tripped case nearly matches the predictions (within 15%) over the entire body flap, including the location of the reattachment heating. These comparisons suggest that laminar, transitional, and turbulent heating levels have been obtained for the nominal deflected body-flap case of 20 deg in the 31-Inch Mach 10 Air Tunnel. Other body-flap deflections were also tested, although computational results from LAURA were not available for these cases.

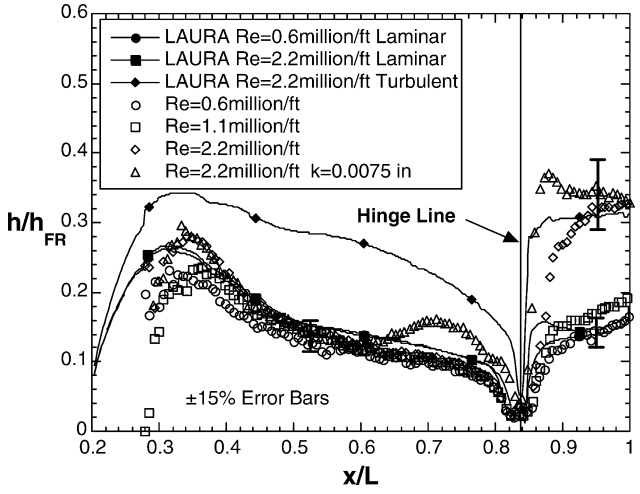

a) Longitudinal distribution at BF-Station

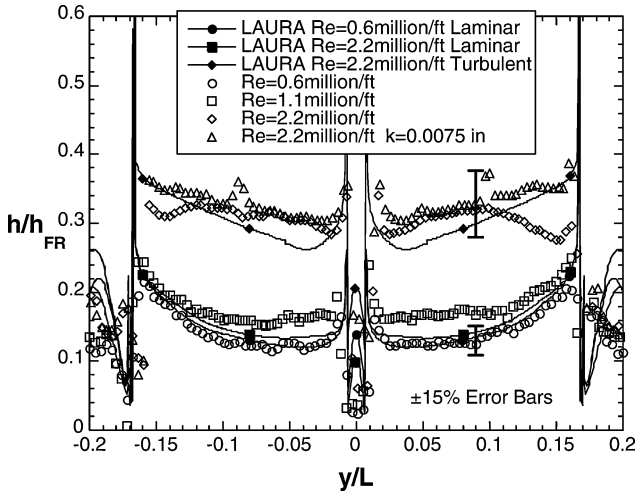

b) Spanwise distribution at SW-Station 3

Fig. 10 Comparisons of heating results to predictions for $M_\infty = 10$, $\alpha = 40$ deg, and $\delta_{BF} = 20$ deg.

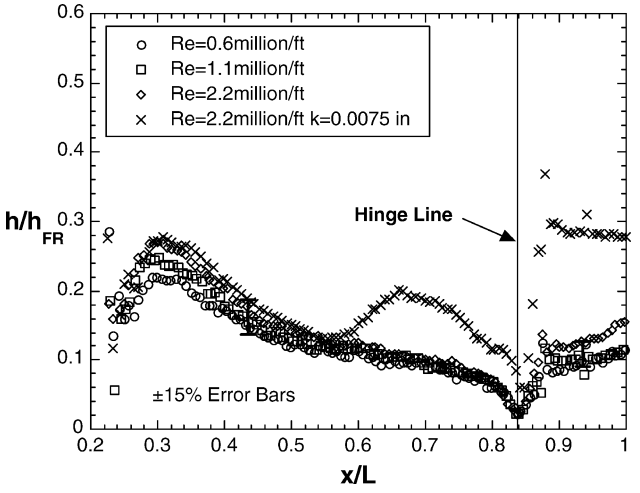

a) Longitudinal distribution at BF-Station

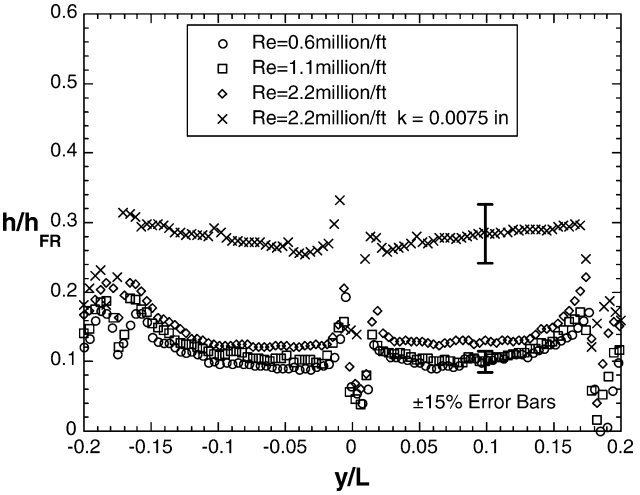

b) Spanwise distribution at SW-Station 3

Fig. 11 Comparisons of heating results for $M_\infty = 10$, $\alpha = 40$ deg, and $\delta_{BF} = 15$ deg.

Figures 11 and 12 provide the experimental body-flap heating levels for the $\delta_{BF} = 15$ and 25 deg cases, respectively. For the lowest body-flap deflection tested (Fig. 11), flow over the body flap appears laminar for all three Reynolds numbers without the trips as the heating distributions roughly collapse, whereas the tripped case nearly triples the heating level on the body flap. As shown in Fig. 12, for $\delta_{BF} = 25$ deg the heating on the body flap increased with Reynolds number for the untripped cases with the 0.0236 scale model; the tripped result closely matches the highest-Reynolds-number case on the body flap.

To establish that laminar heating levels were obtained on the body flap, a limited number of runs were conducted with the 0.0177-scale model, and these results are also included in Fig. 12. Note that the two $Re = 0.6 \times 10^6$/ft cases are within the experimental scatter of each other, which might be an indication that the heating levels on the body flap are laminar for these cases. As further evidence that the flow is laminar for these cases, experimental surface streamlines in the vicinity of the body flap for $\delta_{BF} = 25$ deg and $Re = 1.1 \times 10^6$/ft are presented in Fig. 13. This oil-flow photograph was from an earlier test entry in the 31-Inch Mach 10 Tunnel (for a very limited combination of α, Re, and δ_{BF} with a 0.0177-scale Rev 3.1 model of the X-38). These surface streamlines can be qualitatively compared to the computed streamlines, shown in Figs. 14a and 14b for the laminar ($Re = 0.6 \times 10^6$/ft) and turbulent ($Re = 2.2 \times 10^6$/ft) cases, respectively. Even though the body-flap deflection angles are not the same between Figs. 13 and 14, the experimental results, in terms of the extent of separation, the location of reattachment, the highly

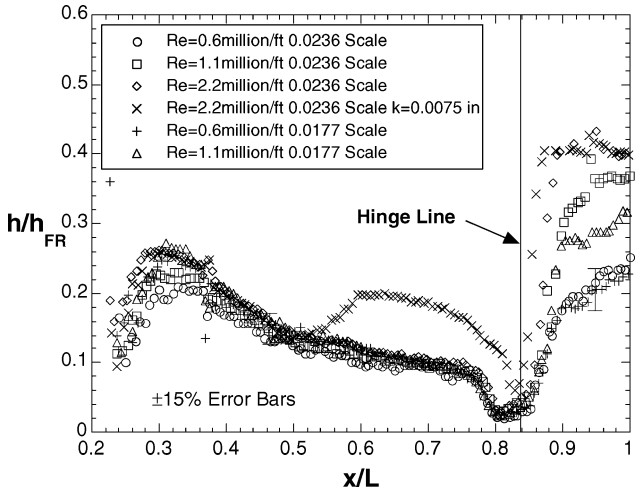

a) Longitudinal distribution at BF-Station

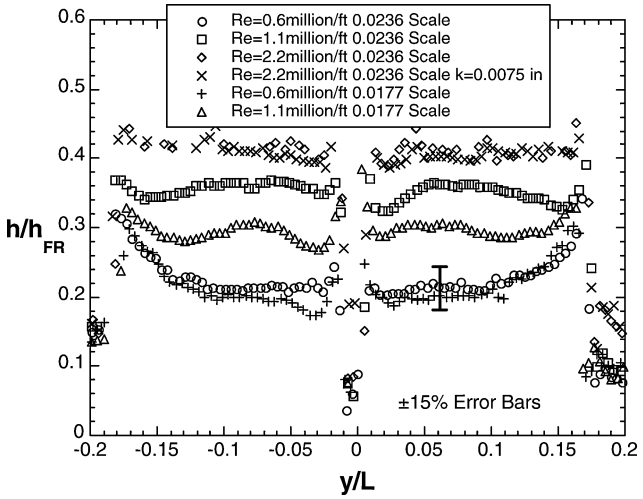

b) Spanwise distribution at SW-Station 3

Fig. 12 Comparisons of heating results for $M_\infty = 10$, $\alpha = 40$ deg, and $\delta_{BF} = 25$ deg.

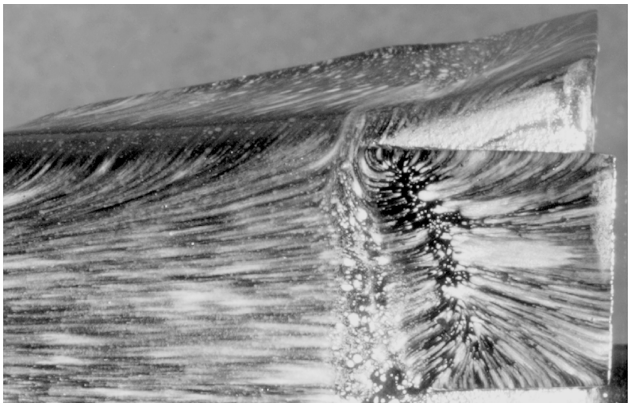

Fig. 13 Experimental surface streamlines for $\alpha = 40$ deg, $Re = 1.1 \times 10^6$/ft, and $\delta_{BF} = 25$ deg.

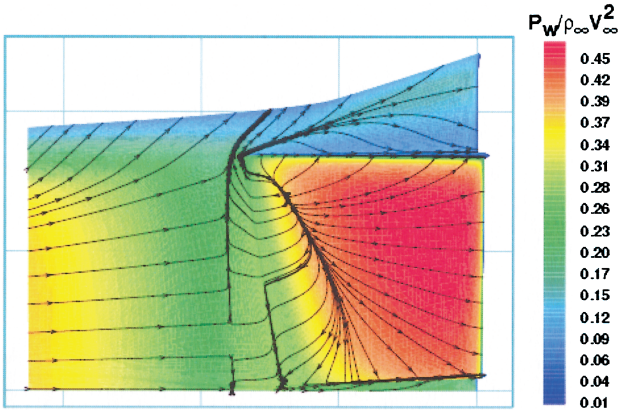

Fig. 14a Surface streamlines and pressures from laminar predictions for $\alpha = 40$ deg, $Re = 0.6 \times 10^6$/ft, and $\delta_{BF} = 20$ deg.

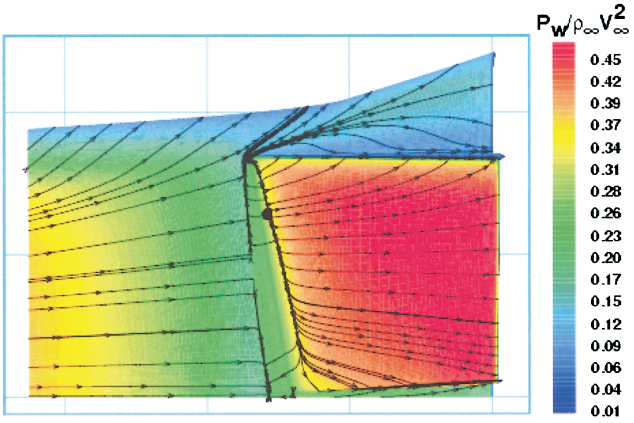

Fig. 14b Surface streamlines and pressures from turbulent predictions for $\alpha = 40$ deg, $Re = 2.3 \times 10^6$/ft, and $\delta_{BF} = 20$ deg.

curved flow toward the outboard regions of the flap, more closely resemble the streamlines of the laminar solution.

The X-38 body-flap design heating environment for flight is being defined by the program mainly based on experimental results obtained in the 20-Inch Mach 6 Tunnel. Reference 18 has presented an overview of these earlier LaRC studies. A comparison of the present measurements at Mach 10 to the Mach 6 results, in terms of heating on the body flap as referenced to a laminar value on the forebody, is provided in Fig. 15. The Mach 6 measurements shown in Fig. 15 include early results that have been provided to the program and more recently measured results not yet reported. Although the turbulent/tripped results between the two tunnels are shown to have excellent agreement, the original results from the

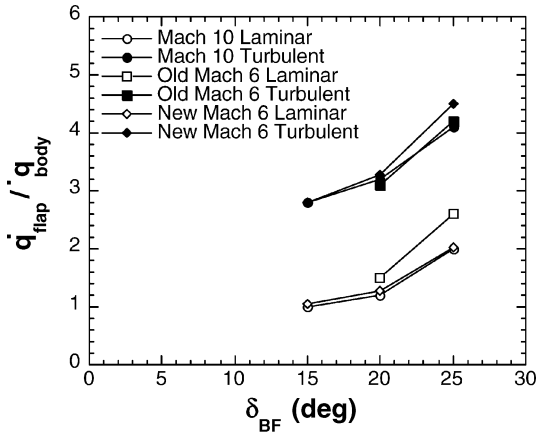

Fig. 15 Body-flap heating referenced to laminar forebody heating ahead of separation for $\alpha = 40$ deg.

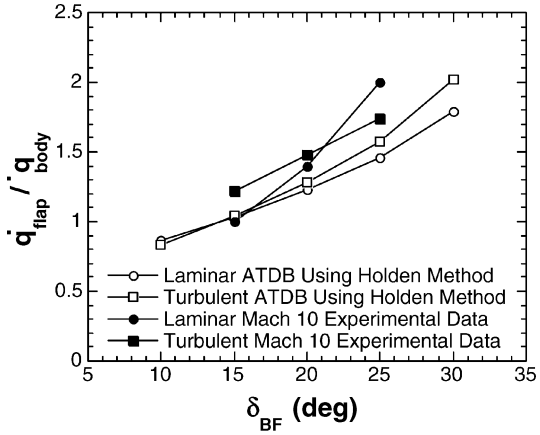

Fig. 16 Comparison of Mach 10 body-flap heating referenced to forebody heating ahead of separation against X-38 ATDB using Holden's method.

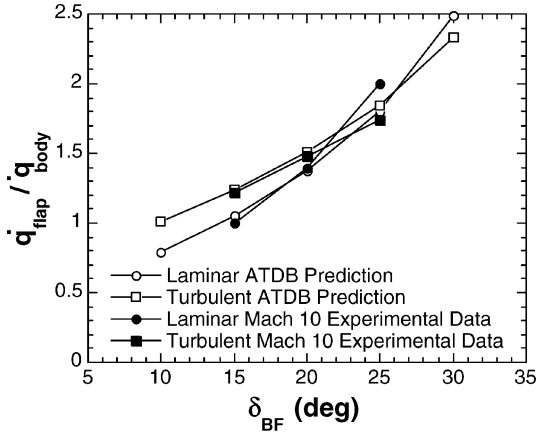

Fig. 17 Comparison of Mach 10 body-flap heating referenced to forebody heating ahead of separation against X-38 ATDB using current method.

Mach 6 tunnel that were thought to be laminar are slightly higher than the Mach 10 results. The earlier Mach 6 tunnel entry utilized the 0.0295-scale model and did not obtain data at the lowest Reynolds number available in the tunnel. The more recent Mach 6 results utilized the 0.0177-scale model, and many runs at a low enough Reynolds number to ensure laminar heating levels agreed well on the body flap. The newer Mach 6 results shown in Fig. 15 more closely match the Mach 10 results, which provides stronger evidence of the validity of the laminar, transitional, and turbulent results provided to the X-38 program.

Currently, the nominal body-flap deflection angle required to trim the vehicle in hypersonic flight is smaller than the deflections tested in the aeroheating studies performed in the LaRC 20-In Mach 6 Air Tunnel and incorporated in the body-flap design specification. To provide body-flap heating at operational deflections, the X-38 ATDB utilizes a correlation technique that takes advantage of the well-documented interdependence between heating and pressure for flows experiencing shock/boundary-layer interactions.[41–46] As noted in these references, there is a power–law relation between the ratio of the peak values of pressure and heating to their undisturbed values that is a function of the boundary-layer state in the vicinity of the interaction. The correlation as currently used is

$$\frac{(\dot{q}/\dot{q}_{\mathrm{Ref}})_{\mathrm{flap}}}{(\dot{q}/\dot{q}_{\mathrm{Ref}})_{\mathrm{body}}} = F\left(\frac{p_{\mathrm{flap}}}{p_{\mathrm{body}}}\right)^{n} \tag{1}$$

where the exponent n (as well as the heating and pressure values) depends on whether the flow is laminar or turbulent and F is a constant that depends on the correlation method. For instance, Ref. 43 has suggested that $n = 0.7$ for laminar heating and $n = 0.85$ for turbulent heating, while $F = 1$. Others have suggested many different combinations of these parameters. The X-38 ATDB is currently using $n = 1.1$ and $F = 1$ for laminar flow, while $n = 0.8$ and $F = 1.2$ for turbulent. Figures 16 and 17 provide a comparison of the laminar and turbulent wind-tunnel results to the predicted body flap heating from the ATDB based on the Holden and ATDB methods, respectively. For this paper the forebody location was selected to be ahead of the separated flow region. The predicted heating results are based on inviscid pressure ratio terms used to calculate the right-hand side of Eq. (1), whereas the wind-tunnel results shown in Figs. 10–12 provide the experimental heating ratio on the left-hand side of Eq. (1). As the trips did not appear to provide fully turbulent flow on the forebody, the turbulent wind-tunnel curves of Figs. 16 and 17 assume the computational value of heating shown in Fig. 10 as the turbulent forebody value. Based on the comparisons shown in Figs. 16 and 17, the correlation method currently employed by the X-38 ATDB provides a better representation of the present Mach 10 experimental data.

Conclusions

A recent effort at the NASA Langley Research Center to extend the experimental aeroheating database on the X-38 Rev 8.3 configuration to higher-Mach-number conditions is presented. Global surface heat-transfer distributions were measured on several scale models of the current X-38 flight vehicle at Mach 10 in air. The primary parametrics investigated include freestream unit Reynolds numbers from 0.6 to 2.2×10^6/ft and body-flap deflections of 15, 20, and 25 deg for an angle of attack of 40 deg. Boundary-layer trips were utilized to ensure turbulent heating levels on the deflected body flaps. The Reynolds-number range available with the Mach 10 facility along with the boundary-layer trips was sufficient to produce laminar, transitional, and turbulent boundary layers on the deflected body flaps. Comparisons of the present experimental results to computational predictions were performed, and agreement within the experimental uncertainty was shown. The body-flap heating was on the order of two times the reference levels under laminar conditions and as much as four times the reference under turbulent conditions. The methodology employed by the X-38 program to predict the in-flight heating levels on the body flap was shown to agree with the Mach 10 experimental data.

References

[1]Brown, D., "Manning the Lifeboats on the International Space Station," *Launchspace*, Vol. 3, No. 2, 1998, pp. 20–22.

[2]Asker, J. R., "For Myriad Woes, NASA Calls X-38 to the Rescue," *Aviation Week and Space Technology*, Vol. 145, No. 20, 11 Nov. 1996, pp. 70–71.

[3]Smith, B. A., "Weather May Hamper X-38 Drop Tests," *Aviation Week and Space Technolgy*, Vol. 147, No. 24, 8 Dec. 1997, p. 33.

[4]Kandebo, S. W., "Vista F-16 Tests Preview X-38 Flight Controls," *Aviation Week and Space Technology*, Vol. 149, No. 16, 19 Oct. 1998, p. 41.

[5]Covault, C., "Second X-38 Set for Flight," *Aviation Week and Space Technology*, Vol. 149, No. 9, 31 Aug. 1998, p. 58.

[6]Reed, R. D., "Wingless Flight The Lifting Body Story," NASA SP-4220, 1997.

[7]Barret, C., "Lifting Body Stability and Control," NASA TM-1999-209255, March 1999.

[8]Hallion, R. P. (ed), *The Hypersonic Revolution: Eight Case Studies in the History of Hypersonic Technology*, Vol. 2, Special Staff Office, Aeronautical Systems Div., Wright–Patterson AFB, OH, 1987, pp. 893–923.

[9]Dornhiem, M. A., "X-38 Transitions from Lifting Body to Parafoil," *Aviation Week and Space Technology*, Vol. 148, No. 12, 23 Mar. 1998, p. 92.

[10]Labbe, S. G., Perez, L. F., Fitzgerald, S. M., Longo, J. M. A., and Rapuc, M., "X-38 NASA/DLR/ESA-Dassault Aviation Integrated Aerodynamic and Aerothermodynamics Activities," *Proceedings of the Atmospheric Reentry Vehicle and Systems International Symposium*, French Association for Aeronautics and Astronautics, Arachon, France, 1999.

[11]Tribot, J. P., "X-38 Step 2 Aerothermodynamic Data Base," Dassault Aviation Document, DGT 77469, Jan. 1999.

[12]Tribot, J. P., Tran, P., Pallegoix, J. F., Orlowski, M., Bruck, S., Andres, O. P., and Fitzgerald, S. M., "X-38 Aerothermodynamics," *Proceedings of the Atmospheric Reentry Vehicle and Systems International Symposium*, French Association for Aeronautics and Astronautics, Arachon, France, 1999.

[13]Campbell, C. H., Caram, J. M., Berry, S. A., Horvath, T. J., Merski, N. R., Loomis, M. P., and Venkatapathy, E., "An Overview of X-38 Hypersonic Aerothermodynamic Wind Tunnel Data and Comparison with Numerical Results," AIAA Paper 97-2475, June 1997.

[14]Loomis, M. P., Venkatapathy, E., Papadopoulos, P., Davies, C. B., Berry, S. A., Horvath, T. J., and Campbell, C. H., "Aeroheating and Aerodynamic CFD Validation and Prediction for the Computational/Experimental Aeroheating Predictions for the X-38 Program," AIAA Paper 97-2478, June 1997.

[15]Berry, S. A., Horvath, T. J., Roback, V. E., and Williams, G. B., "Results of Aerothermodynamic and Boundary-Layer Transition Testing of 0.0362-Scale X-38 (Rev. 3.1) Vehicle in NASA Langley 20-Inch Mach 6 Tunnel," NASA TM-112857, Sept. 1997.

[16]Berry, S. A., Bouslog, S. A., Brauckmann, G. J., and Caram, J. M., "Shuttle Orbiter Experimental Boundary-Layer Transition Results with Isolated Roughness," *Journal of Spacecraft and Rockets*, Vol. 35, No. 3, 1998, pp. 241–248.

[17]Campbell, C. H., Caram, J. M., Berry, S. A., Horvath, T. J., and DiFulvio, M., "Overview of X-38 Hypersonic Wind Tunnel Data and Comparison with Numerical Results," AIAA Paper 97-0567, Jan. 1997.

[18]Horvath, T. J., Berry, S. A., Merski, N. R., and Fitzgerald, S. M., "X-38 Experimental Aerothermodynamics," *Journal of Spacecraft and Rockets*, Vol. 41, No. 2, 2004, pp. 272–292.

[19]Muhlrazer, A., Frohlich, A., and Wildenrotter, K., "Design, Material and Manufacturing Aspects of the X-38 Body Flaps," *Proceedings of the Atmospheric Reentry Vehicle and Systems International Symposium*, French Association for Aeronautics and Astronautics, Arachon, France, 1999.

[20]Trabandt, U., Schmid, T., Reinkober, H., and Ritter, H., "Light-Weight CMC TPS for Future RLV Applied on X-38 Nose Skirt," *Proceedings of the Atmospheric Reentry Vehicle and Systems International Symposium*, French Association for Aeronautics and Astronautics, Arachon, France, 1999.

[21]Campbell, C. H., Caram, J. M., Li, C. P., and Madden, C. M., "Aerothermodynamic Environment Definition for an X-23/X-24A Derived Assured Crew Return Vehicle," AIAA Paper 96-1862, 1996.

[22]Miller, C. G., "Langley Hypersonic Aerodynamic/Aerothermodynamic Testing Capabilities—Present and Future," AIAA Paper 90-1376, June 1990.

[23]Micol, J. R., "Hypersonic Aerodynamic/Aerothermodynamic Testing Capabilities at Langley Research Center: Aerothermodynamic Facilities Complex," AIAA Paper 95-2107, June 1995.

[24]Buck, G. M., "Automated Thermal Mapping Techniques Using Chromatic Image Analysis," NASA TM-101554, April 1989.

[25]Buck, G. M., "Surface Temperature/Heat Transfer Measurement Using a Quantitative Phosphor Thermography System," AIAA Paper 91-0064, Jan. 1991.

[26]Merski, N. R., "Reduction and Analysis of Phosphor Thermography Data with the IHEAT Software Package," AIAA Paper 98-0712, Jan. 1998.

[27]Fay, J. A., and Riddell, F. R., "Theory of Stagnation Point Heat Transfer in Dissociated Air," *Journal of the Aerospace Sciences*, Vol. 25, No. 2, 1958, pp. 73–85, 121.

[28]Gnoffo, P. A., Gupta, R. N., and Shinn, J., "Conservation Equations and Physical Models for Hypersonic Air Flows in Thermal and Chemical Nonequilibrium," NASA TP-2867, Feb. 1989.

[29]Gnoffo, P. A., "Upwind-Biased, Point-Implicit Relaxation Strategies for Viscous Hypersonic Flows," AIAA Paper 89-1972, June 1989.

[30]Gnoffo, P. A., "An Upwind Point Implicit Relaxation Algorithm for Viscous Compressible Perfect-Gas Flows," NASA TP-2953, Feb. 1990.

[31]Roe, P. L., "Approximate Riemann Solvers, Parameter Vectors, and Difference Schemes," *Journal of Computational Physics*, Vol. 43, No. 2, 1981, pp. 357–372.

[32]Harten, A., "High Resolution Schemes for Hyperbolic Conservation Laws," *Journal of Computational Physics*, Vol. 49, No. 2, 1983, pp. 357–393.

[33]Yee, H. C., "On Symmetric and Upwind TVD Schemes," NASA TM-86842, Sept. 1985.

[34]Wilcox, D. C., "Turbulence Modeling for CFD," DCW Industries, Inc., La Canada, CA, 1993.

[35]Steinbrenner, J. P., Chawner, J. R., and Fouts, C. L., "The GRIDGEN 3D Multiple Block Grid Generation System," Wright Research and Development Center, Rept. WRDC-TR-90-3022, Wright–Patterson AFB, OH, Oct. 1989.

[36]Alter, S. J., "The Volume Grid Manipulator (VGM): A Grid Reusability Tool," NASA CR-4772, April 1997.

[37]Sorenson, R. L., and Alter, S. J., "3DGRAPE/AL: The Ames/Langley Technology Upgrade," NASA CP-3291, May 1995, pp. 447–462.

[38]Weilmuenster, K. J., Gnoffo, P. A., Greene, F. A., Riley, C. J., and Hamilton, H. H., II, "Hypersonic Thermal Environment of a Proposed Single-Stage-to-Orbit Vehicle," *Journal of Spacecraft and Rockets*, Vol. 34, No. 6, 1997, pp. 697–704.

[39]Gnoffo, P. A., Weilmuenster, K. J., and Alter, S. J., "Multiblock Analysis for Shuttle Orbiter Reentry Heating from Mach 24 to Mach 12," *Journal of Spacecraft and Rockets*, Vol. 31, No. 3, 1994, pp. 367–377.

[40]Weilmuenster, K. J., and Gnoffo, P. A., "Solution Strategy for Three-Dimensional Configurations at Hypersonic Speeds," *Journal of Spacecraft and Rockets*, Vol. 30, No. 4, 1993, pp. 385–394.

[41]Neumann, R. D., "Special Topics in Hypersonic Flow," *Aerodynamic Problems of Hypersonic Vehicle*, LS-42-Vol. 1, AGARD, July 1972, pp. 7-1–7-64.

[42]Holden, M. S., "Shock Wave Turbulent Boundary Layer Interaction in Hypersonic Flow," AIAA Paper 72-74, Jan. 1972.

[43]Holden, M. S., "A Study of Flow Separation in Regions of Shock Wave Boundary Layer Interaction in Hypersonic Flow," AIAA Paper 78-1169, July 1978.

[44]Hung, F. T., "Interference Heating due to Shock Wave Impingements on Laminar Boundary Layers," AIAA Paper 73-678, July 1973.

[45]Hung, F. T., "Three-Dimensional Shock Wave Interference Heating Prediction," AIAA Paper 77-756, July 1977.

[46]Simeonides, G., "Hypersonic Shock Wave Boundary Layer Interactions over Simplified Deflected Control Surface Configurations," *Special Course on Shock-Wave/Boundary-Layer Interactions in Supersonic and Hypersonic Flows*, Rept. 792, AGARD, Aug. 1993.

M. Torres
Associate Editor

Color reproductions courtesy of NASA Langley Research Center.